



## Titan imagery with Keck adaptive optics during and after probe entry

Imke de Pater,<sup>1</sup> Máté Ádámkóvics,<sup>1</sup> Antonin H. Bouchez,<sup>2</sup> Michael E. Brown,<sup>3</sup> Seran G. Gibbard,<sup>4</sup> Franck Marchis,<sup>1</sup> Henry G. Roe,<sup>3</sup> Emily L. Schaller,<sup>3</sup> and Eliot Young<sup>5</sup>

Received 21 October 2005; revised 1 March 2006; accepted 9 March 2006; published 22 June 2006.

[1] We present adaptive optics data from the Keck telescope, taken while the Huygens probe descended through Titan's atmosphere and on the days following touchdown. No probe entry signal was detected. Our observations span a solar phase angle range from  $0.05^\circ$  up to  $0.8^\circ$ , with the Sun in the west. Contrary to expectations, the east side of Titan's stratosphere was usually brightest. Compiling images obtained with Keck and Gemini over the past few years reveals that the east-west asymmetry can be explained by a combination of the solar phase angle effect and an enhancement in the haze density on Titan's morning hemisphere. While stratospheric haze was prominent over the northern hemisphere, tropospheric haze dominated the south, from the south pole up to latitudes of  $\sim 45^\circ\text{S}$ . At  $2.1\ \mu\text{m}$  this haze forms a polar cap, while at  $1.22\ \mu\text{m}$  it appears in the form of a collar at  $60^\circ\text{S}$ . A few small clouds were usually present near the south pole, at altitudes of 30–40 km. Our narrowband J,H,K images of Titan's surface compare extremely well with that obtained by Cassini ISS, down to the small-scale features. The surface contrast between dark and bright areas may be larger at  $2\ \mu\text{m}$  than at  $1.6$  and  $1.3\ \mu\text{m}$ , which would imply that the dark areas may be covered by a coarser-grained frost than the bright regions and/or that there is additional  $2\ \mu\text{m}$  absorption there.

**Citation:** de Pater, I., M. Ádámkóvics, A. H. Bouchez, M. E. Brown, S. G. Gibbard, F. Marchis, H. G. Roe, E. L. Schaller, and E. Young (2006), Titan imagery with Keck adaptive optics during and after probe entry, *J. Geophys. Res.*, *111*, E07S05, doi:10.1029/2005JE002620.

### 1. Introduction

[2] On 14 January 2005, at 10:13 UTC, the Huygens probe entered Titan's atmosphere. Almost 2.5 hours later, at 12:34 UTC, it touched down on the satellite's surface where it remained operational for another hour and 12 minutes. The timing and viewing geometry of the event were excellent for observatories on Mauna Kea, Hawaii. We observed Titan with the adaptive optics system on the 10-m Keck telescope to characterize/monitor the weather while the probe glided down through its atmosphere. Our data form part of a long-term monitoring program of Titan carried out by several groups at different 8–10-m sized telescopes. The data taken near probe entry time are particularly valuable in this data set because it allows models of ground-based observations to be tested with “ground-truth”

data taken by the probe during its descent (e.g., temperature-pressure profile, winds, hazes, clouds).

### 2. Observations and Data Processing

[3] We observed Titan with the 10-m W.M. Keck II telescope on UT 14–17 January 2005. We used the adaptive optics (AO) system with the facility Near-Infrared Camera NIRC2, which has a  $1024 \times 1024$  Aladdin-3 InSb detector array. We used NIRC2 in high angular resolution mode,  $9.94 \pm 0.03$  mas per pixel (<http://www2.keck.hawaii.edu/inst/nirc2/genspecs.html>; pixel size confirmed by de Pater *et al.* [2006]), which translates to 58.2 km/pixel on Titan. In addition to broadband and narrowband imaging, we took low-resolution spectra in H ( $1.582$ – $1.749\ \mu\text{m}$ ) and K' ( $1.999$ – $2.221\ \mu\text{m}$ ) bands at a spectral resolution  $R = \lambda/\Delta\lambda \approx 1600$ – $1700$ , where  $\lambda$  is the wavelength. A detailed log of the observations is provided in Table 1. We note that on 14 January the weather at the telescope was far from optimal with winds reaching over 35 mph. The data quality on this day is therefore lower than usual. The approximate altitudes probed by the various filters are summarized in Figure 5, and discussed in section 4.

[4] All images were processed using standard near-infrared data reduction techniques (flat-fielded, sky-subtracted, with bad pixels replaced by the median of surrounding pixels). We typically obtained a spatial resolution

<sup>1</sup>Department of Astronomy, University of California, Berkeley, California, USA.

<sup>2</sup>Caltech Optical Observatories, California Institute of Technology, Pasadena, California, USA.

<sup>3</sup>Division of Geological and Planetary Sciences, California Institute of Technology, Pasadena, California, USA.

<sup>4</sup>Lawrence Livermore National Laboratory, Livermore, California, USA.

<sup>5</sup>Southwest Research Institute, Boulder, Colorado, USA.

**Table 1.** Log of Titan Observations in January 2005<sup>a</sup>

UT Time, <sup>b</sup> day-hr:min <sup>b</sup>	I/S <sup>c</sup>	Filter	Wavelength Range, $\mu\text{m}$	No. Frames <sup>d</sup> $\times$ sec	CML, <sup>e</sup> deg	Phase Angle, <sup>f</sup> deg	Calibration <sup>g</sup> Factor $\rightarrow$ $I/F$	Titan's $I/F$
14-09:59	I	CH <sub>4</sub> L	1.613–1.749	80 $\times$ 10	156.6	0.047	9.67 e-5	0.015
14-11:16	I	K'	1.948–2.299	4 $\times$ 10	157.8	0.054	7.50e-5	0.033
14-11:28	I	H <sub>2(v=1-0)</sub>	2.111–2.145	4 $\times$ 30	158.0	0.055	1.0e-3 <sup>h</sup>	0.023
15-07:00	I	K'	1.948–2.299	4 $\times$ 30	176.5	0.154	8.07e-5	0.024
15-07:30	I	J	1.166–1.330	3 $\times$ 30	176.9	0.156	6.57e-5	0.053
15-07:36	I	H <sub>2(v=1-0)</sub>	2.111–2.145	3 $\times$ 60	177.0	0.157	1.37e-3	0.0237
15-07:43	I	H	1.485–1.781	3 $\times$ 30	177.1	0.157	4.19e-5	0.028
15-07:48	I	HeIB	2.040–2.072	3 $\times$ 60	177.2	0.158	1.26e-3	0.0643
15-07:53	I	Bry	2.152–2.185	3 $\times$ 60	177.3	0.158	1.44e-3	0.0120
15-07:58	I	CH <sub>4</sub> L	1.613–1.749	3 $\times$ 30	177.4	0.159	1.02E-4	0.0125
15-08:03	I	FeII	1.633–1.658	3 $\times$ 60	177.5	0.159	5.52e-4	0.01320
15-08:08	I	Hcont	1.569–1.592	3 $\times$ 30	177.6	0.159	1.41e-3	0.171
15-08:13	I	Pa $\beta$	1.281–1.300	3 $\times$ 30	177.6	0.160	1.33e-3	0.259
15-08:17	I	Jcont	1.203–1.233	3 $\times$ 30	177.7	0.160	1.56e-3	0.0955
15-08:22	I	Kcont	2.256–2.285	3 $\times$ 60	177.7	0.161	2.34e-3	0.0069
15-08:28	I	CO <sub>v=2-0</sub>	2.276–2.302	3 $\times$ 60	177.9	0.161	2.87e-3	0.0065
15-09:37	I	K'	1.948–2.299	25 $\times$ 5	178.9	0.167	8.07e-5	
15-09:37	S	K'	1.948–2.299	25 $\times$ 120	178.9	0.167		
16-10:40	I	K'	1.948–2.299	3 $\times$ 30	202.6	0.294	6.33e-5	0.0265
16-10:48	I	H <sub>2(v=1-0)</sub>	2.111–2.145	4 $\times$ 60	202.7	0.295	9.90E-4	0.0240
16-10:55	I	Bry	2.152–2.185	3 $\times$ 60	202.8	0.296	1.07E-3	0.0114
16-11:06	I	FeII	1.633–1.658	3 $\times$ 60	203.0	0.296	4.83e-4	0.0149
16-11:14	I	CH <sub>4</sub> L	1.613–1.749	4 $\times$ 30	203.2	0.297	8.64e-5	0.0144
16-11:52	I	H	1.485–1.781	19 $\times$ 5	203.7	0.300	3.66e-5	0.0324
16-11:52	S	H	1.485–1.781	19 $\times$ 120	203.7	0.300		
17-10:40	I	K'	1.948–2.299	4 $\times$ 30	225.3	0.415	6.40e-5	0.0261
17-10:46	I	H <sub>2(v=1-0)</sub>	2.111–2.145	3 $\times$ 60	225.4	0.416	1.00e-3	0.02326
17-10:52	I	Bry	2.152–2.185	3 $\times$ 60	225.5	0.416	1.08e-3	0.0113
17-10:58	I	FeII	1.633–1.658	3 $\times$ 60	225.6	0.417	4.73e-4	0.0138
17-11:03	I	CH <sub>4</sub> L	1.613–1.749	3 $\times$ 30	225.7	0.417	8.60e-5	0.0132
17-11:08	I	H	1.485–1.781	3 $\times$ 30	225.8	0.418	3.60e-5	0.0292
17-11:54	I	K'	1.948–2.299	19 $\times$ 5	226.5	0.422	6.40e-5	
17-11:54	S	K'	1.948–2.299	19 $\times$ 120	226.5	0.422		
17-13:32	I	H	1.485–1.781	4 $\times$ 5	228.0	0.430	3.60e-5	
17-13:32	S	H	1.485–1.781	4 $\times$ 120	228.0	0.430		

<sup>a</sup>For all observations, the geocentric distance  $\Delta \approx 8.068 - 8.086$  AU; heliocentric distance  $r_0 \approx 9.053 - 9.064$  AU; angular diameter is  $0.88''$ ; position angle of north pole  $PA = 353.33^\circ$  (all images are rotated so Titan north is up).

<sup>b</sup>Approximate starting time (UT).

<sup>c</sup>I for images; S for spectra.

<sup>d</sup>Number of images times the integration time in seconds.

<sup>e</sup>Central Meridian Longitude (or sub-Earth longitude).

<sup>f</sup>Angle Sun-Titan-Earth; Sun is to the west of Titan on the sky.

<sup>g</sup>Factor with which to multiply a 1 second exposure image to convert to  $I/F$ .

<sup>h</sup>No photometric calibration was done; we adopted the values as listed, in analogy with other nights.

(FWHM) of  $\sim 0.05''$  in K' band, and  $\sim 0.04''$  in J and H band. Strehl ratios (the ratio of the peak intensity of the observed point spread function (PSF) to the theoretical maximum for the telescope aperture) were  $\sim 0.35-0.50$  in K',  $\sim 0.4$  in H, and  $\sim 0.1-0.2$  in J band.

[5] Photometric calibrations were performed on the stars HD22686 and HD129655 [Elias *et al.*, 1982]. These measurements were used to derive the conversion factors in Table 1, with which to multiply the images (in cts/sec) to convert them to  $I/F$ .  $I$  is the intensity reflected by Titan at the wavelength observed, and  $\pi F$  is the solar flux received by Titan at the same wavelength [Colina *et al.*, 1996a]. The total  $I/F$  equals the geometric albedo when viewed at zero phase angle. The observed disk-averaged  $I/F$  in each filter is tabulated in Table 1.

[6] In addition to the basic-processed images, we also present images sharpened with a deconvolution algorithm. We used AIDA, an Adaptive Image Deconvolution Algorithm (E. F. Y. Hom *et al.*, AIDA: An Adaptive Image Deconvolution Algorithm with application to multi-frame and 3D data, submitted to *Journal of Optical Society of*

*America A*, 2006.), which is similar to MISTRAL, a Myopic Iterative STep-preserving Restoration ALgorithm, especially aimed at AO observations of planetary objects [Mugnier *et al.*, 2004]. MISTRAL and AIDA use a stochastic approach to find the best image reconstruction, using information both about the object and the PSF. The main improvement in the AIDA algorithm to date is its speed and an automatic search for the best regularization parameters (it is about 200 times faster than MISTRAL).

[7] To check the reliability of the algorithm, we constructed two simulated images of Titan via slight modifications to the Gibbard *et al.* [1999] models, constructed to simulate Keck images of Titan obtained via speckle interferometry. Model 1 consists of a disk with a surface albedo of  $\sim 0.04$  and atmosphere with a north-south gradient, and east-west asymmetry. This model is analogous to Titan observed through a stratosphere probing filter, as, e.g., FeII or Bry. Model 2 is more analogous to Titan probed through a broad K-band filter. We added a relatively bright feature on Titan's surface. On both model images, we added Poisson noise (signal to noise is  $\sim 150:1$ ) and convolved

the model with a PSF (image of an observed star). We deconvolved these models with AIDA to address how well surface features and limb brightening characteristics are recovered (see F. Marchis et al. (Shape, size and multiplicity of main-belt asteroids. I. Keck adaptive optics survey, submitted to *Icarus*, 2006) for more deconvolution reality checks, in particular with respect to shape and size of objects).

[8] Results of our deconvolution tests are summarized in Figure 1. Images are shown in the top panels: (1) the original images, (2) after addition of Poisson noise and convolution with a PSF, and (3) the AIDA deconvolved maps. All data were normalized to the disk-averaged value of the original images. The bottom panels show scans through the images, approximately along the horizontal and vertical lines on the images. The surface feature in Model 2 was easily recovered, as well as the limb brightening east-west and north-south. In Model 1 the limb brightening is very steep, and is recovered only partially via deconvolution. This, however, is not surprising, since structure at spatial scales considerably smaller than the diffraction limit of the telescope (approximately the core of the PSF) cannot be recovered. We further see that the sharp edge of the disk is indeed recovered well, as advertised for these algorithms.

[9] Spectra of Titan were obtained in H and K' bands by stepping the spectrometer slit across Titan. While stepping across the satellite, we shifted Titan up and down along the slit, so the sky would be removed by subtraction of adjacent observations. All data were flatfielded, and bad pixels were replaced by the median of surrounding pixels. Wavelength calibration was based on OH lines from the Earth's atmosphere [Rousselot et al., 2000]. In order to correct for telluric absorption and the instrumental transmission function, we observed A and G-type stars. The A stars were divided by the spectrum of Vega (spectral type A0 V [Colina et al., 1996b]), and multiplied by a solar blackbody spectrum. The Titan spectra were then divided by the transmission function derived from these spectra. Finally, the spectra were absolutely calibrated using narrowband images that cover a fraction of the spectrum. In particular, we used FeII images to calibrate the H band spectra, and both the  $H_{2(\nu=1-0)}$  and Bry (average scaling factor) to calibrate K' band.

### 3. Titan During Probe Entry

[10] During the time the Huygens probe descended through Titan's atmosphere we took a sequence of 80 images, 10 seconds each, in the CH<sub>4</sub>L filter. This filter is ideal for these measurements, since it probes primarily Titan's stratosphere, and yet is broader than the conventional narrowband filters that probe this region, providing a higher signal-to-noise (Figure 5). The observations started at 10:01:08.5 UT, and continued through 10:20. Time-averaged images of Titan through all three filters are shown in Figures 2a–2c, with the viewing geometry in Figure 2d. We indicate the approximate position of the Huygens probe landing spot on one of the images.

[11] Probe entry time (passing the 1270 km altitude in Titan's atmosphere) was at 10:13 UT (all times are referenced to receiving time on Earth). At 10:17, when

the probe was at an altitude of 180 km, the parachute was deployed. One minute later, from an altitude of 160 km, Huygens began to transmit radio signals to the Cassini spacecraft, which were detected on Earth by a network of radio telescopes [Bird et al., 2005]. Most of the probe's kinetic energy was expected to be released at altitudes between 400 and 250 km, around 10<sup>h</sup>:16<sup>m</sup> [Lorenz, 2002; Lorenz et al., 2006]. To search for a possible entry flash in our stack of 80 CH<sub>4</sub>L images, we first subtracted the time-averaged image (Figure 2c) from each frame. We did not remove cosmic rays or "hot" pixels from the frames, to avoid removing any potential entry flash signal. We searched for the peak intensity within a 15 × 15 pixel box, encompassing the entire probe entry track. Because this night was not particularly photometric, we subtracted the median background from this peak intensity, where the median intensity was calculated over a box twice as large. Under ideal circumstances this intensity is close to zero, since the time-averaged image was already subtracted. The result is shown in Figure 3, a graph of the peak intensity as a function of time (in minutes after 10:00 UT). The 3-σ RMS value is 0.8 μJy. Hence no signal over 0.8 μJy relative to the average background signal of 0.75 μJy has been detected. This signal thus refers to the upper limit of an entry flash within a single pixel (0.01 × 0.01") over a 10 second integration interval.

[12] Lorenz et al. [2006] predicted (in retrospect) that ground-based telescopes at visible and near-infrared wavelengths might detect an intensity of up to 2.7 μJy, a factor ~3–4 above our upper limit. However, as pointed out by the authors, a large fraction of the radiation was blocked by the probe itself, so perhaps only ~10% of this radiation could have been detected in reality. Additional uncertainties in the various assumptions (e.g., surface area of heat shield) may cause a further decrease in the predicted flux density. So although our upper limit is close to expected detection limits, it is not good enough to constrain potential entry models.

### 4. Haze Profiles and Contribution Functions

[13] Titan's 3-D atmospheric haze distribution can be derived from spectral image data cubes. Adámkóvics et al. [2004] performed such an analysis using Keck AO data obtained in February 2001. We obtained H and K' band image data cubes on 15–17 January (section 2). Although a full analysis of these data will be presented in a future paper, we show a few spectra here to aid in the analysis of our narrowband images. Figure 4a shows H-band spectra from 16 January at the center of the disk, and at latitudes of 50°N and 80°S, i.e., offset from the center by 0.35" to the north and south. These spectra show an enhanced flux density from the north in the stratosphere, at wavelengths  $\lambda \gtrsim 1.63 \mu\text{m}$ . The troposphere is probed at 1.61–1.63 μm. Tropospheric haze is clearly present near the south pole, although at much reduced levels compared to 2001 [see Adámkóvics et al., 2004].

[14] We used Adámkóvics et al.'s [2006] radiative transfer (RT) program to retrieve haze density profiles, which we use below to calculate contribution functions for our narrowband filters. This program is based on Toon et al.'s [1989] two-stream code to simulate the absorption/scatter-

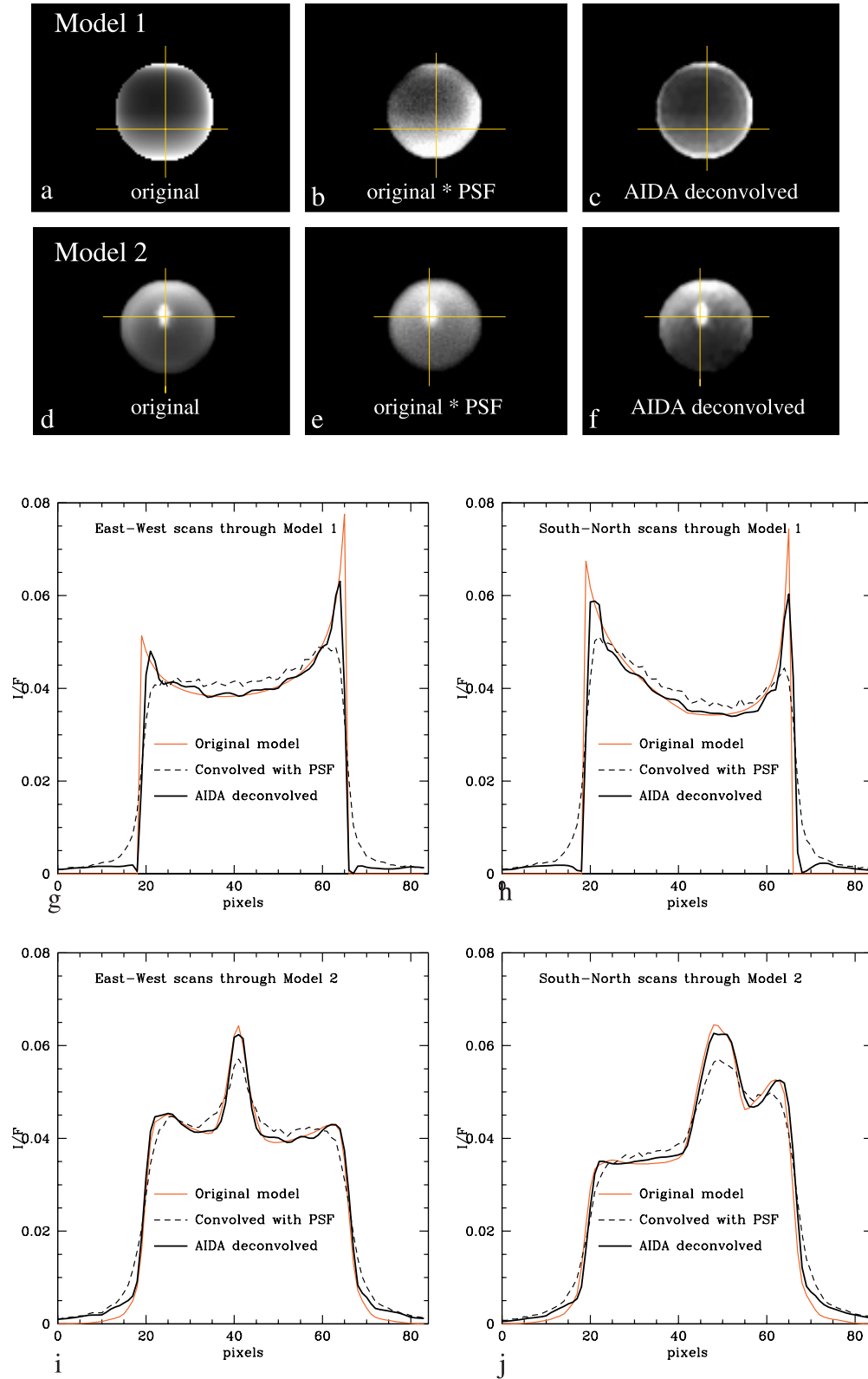


**Figure 1.** Test results of deconvolving artificial Titan images with AIDA. At the top we show (left) the original image, (middle) after adding Poisson noise and convolution with a PSF, and (right) the AIDA deconvolved image. The bottom panels show east-west and north-south scans through these models, approximately along the vertical and horizontal lines on the images.

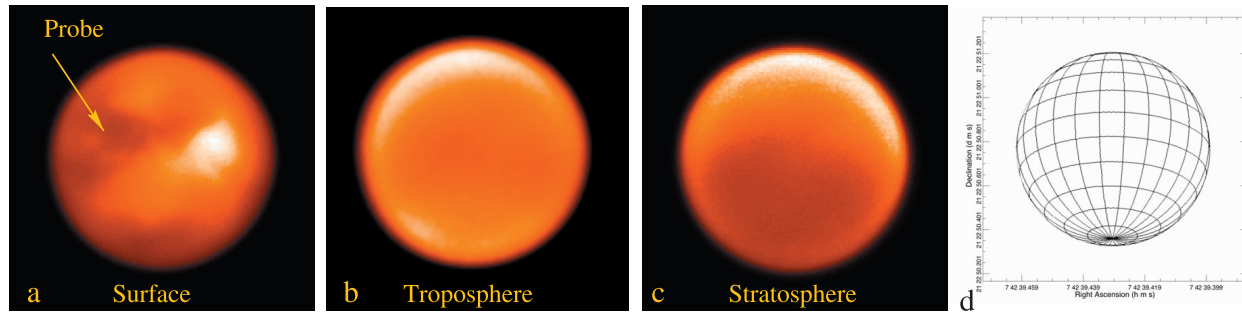


**Figure 2.** Images of (a) Titan’s surface (K’ band), (b) troposphere ( $\text{H}_2(\nu=1-0)$ ), and (c) stratosphere ( $\text{CH}_4\text{L}$ ) during the time the Huygens probe descended through Titan’s atmosphere. The approximate landing site of the probe is indicated by the arrow. (d) The viewing geometry. The latitude and longitude lines are drawn every  $15^\circ$ .

ing of photons in Titan’s atmosphere and reflection of photons from its surface. The optical depth in Titan’s atmosphere is dominated by methane gas absorption and scattering by aerosols. Methane gas absorption is calculated using *Irwin et al.*’s [2005] correlated k-coefficients. We adopt a methane abundance of 5% at the surface, following the saturated vapor curve where appropriate. In the stratosphere we adopt an abundance of 1.6% [Tomasko et al., 2005]. We use *Lellouch et al.*’s [1989] temperature-pressure profile, which is in excellent agreement with that measured in situ by Huygens/HASI [Fulchignoni et al., 2005]. The single scattering albedo was held constant at  $\varpi = 0.95$ . The asymmetry parameter,  $g$ , in the Henyey-Greenstein phase function is a free parameter, usually  $g \sim 0.5-0.7$ .

[15] We show results for two different haze profiles, which both fit the observed spectra equally well. (1) We constrain the haze density to decrease exponentially with a 100 km scale height in the stratosphere, above  $\sim 40$  km, and to be constant below that. These assumptions are consistent with the Huygens probe measurements [Tomasko et al., 2005]. Independent of particle size/properties, we then determine the haze extinction by fitting the observed spectra, starting in the stratosphere at wavelengths where neither the troposphere nor surface are “seen” ( $\lambda > 1.63 \mu\text{m}$  at H,  $\lambda > 2.16 \mu\text{m}$  at K). Next we optimize the fit at shorter wavelengths by including tropospheric haze and surface albedo. The difference in extinction between H and K band is approximately equal to that expected for Mie scattering by  $0.3-0.5 \mu\text{m}$  sized particles. *Adámkovics et al.* [2006] vary  $g$  to fit the extinction in both H and K bands. (2) We also find a best fit to the spectral range that is sensitive to the troposphere by partially clearing the haze in this region from the ground up, which physically could be caused by condensation and rainout [McKay et al., 2001, and references therein]. For these models the haze extinction follows a 32.5 km scale height above 60 km, and is 16.8 km below. Various haze profiles are shown in Figure 4b. Although profile 1 is consistent with the Huygens probe data, profile 2 has been used much in the past, and is a useful approximation to calculate relative atmospheric versus surface contributions, as discussed below.

[16] The two haze profiles are used to determine the approximate altitude range probed in our narrowband filters. To accomplish this, we calculate the contribution functions at each wavelength [see *Adámkovics et al.*, 2006], and

average these over the various filter band passes. Results are shown in Figure 5. As expected, these profiles depend on our atmospheric model, and thus are very different for the two haze profiles, 1 and 2, despite the fact that both profiles give similar fits to the spectra. The reason for this may be caused by shortcomings in the present RT codes, as best illustrated by *Adámkovics et al.*’s [2006] Figure 7. In H band, the model spectrum is too high at wavelengths that probe the troposphere, and at K band the model spectrum “overshoots” the  $I/F$  that might represent the surface. These discrepancies are most likely caused by the inability to properly model weak methane absorption bands in the present RT codes, due, in part, to the fact that not all measured transition frequencies have been assigned, and/or the line intensities are not right. There may also be

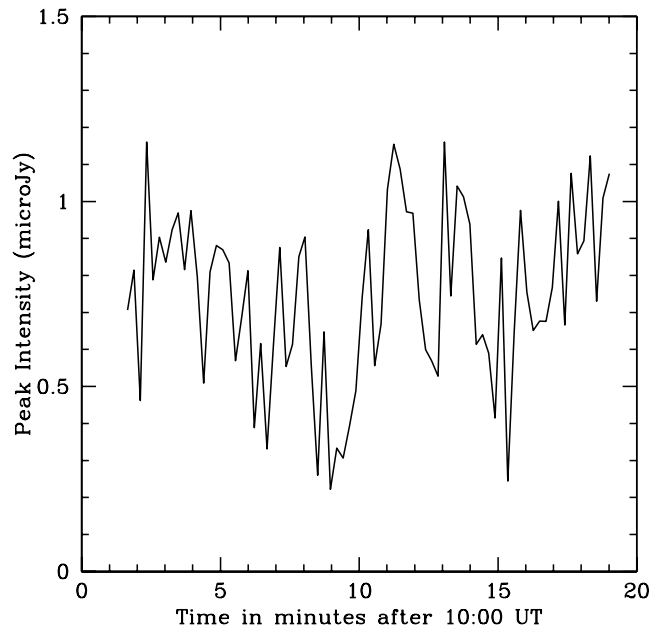


**Figure 3.** Time series of peak intensities in  $\text{CH}_4\text{L}$  images near the probe entry site. No “meteorite” trail is visible above a  $3 - \sigma$  of  $0.8 \mu\text{Jy}$  above the average background of  $0.75 \mu\text{Jy}$ . Probe entry time (passing the 1270 km altitude in Titan’s atmosphere) was at 10:13 UT. At 10:17 the probe passed an altitude of 180 km.

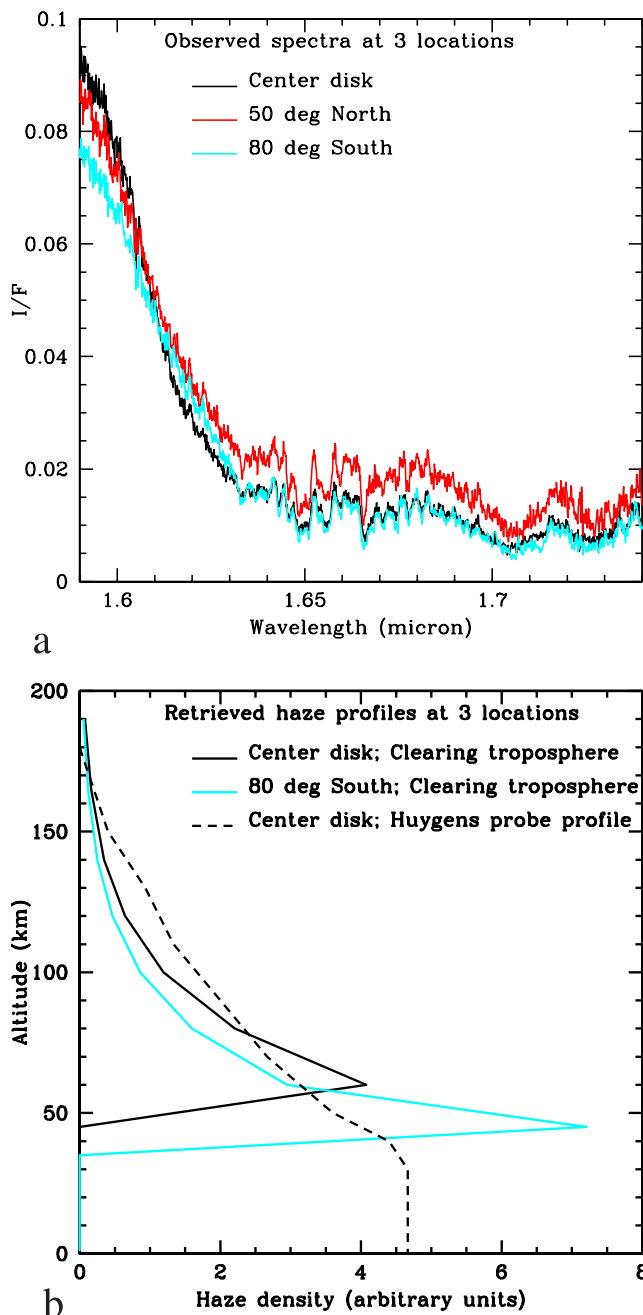


**Figure 4.** (a) Spectra at three locations on Titan’s disk, along the meridian: at the center (latitude  $23^{\circ}\text{S}$ ), in the north ( $50^{\circ}\text{N}$ ), and in the south ( $80^{\circ}\text{S}$ ). (b) Haze density profiles retrieved from the spectra in Figure 4a, using either the tropospheric clearing model (solid lines) or a model with a constant haze profile in the troposphere (dashed line), in analogy with the Huygens probe findings.

additional absorbers in the atmosphere not accounted for in the present RT codes. Since the strong methane bands are properly incorporated by *Irwin et al.*’s [2005] correlated  $k$ -coefficients, Titan’s stratosphere is properly modeled. Weak absorption bands allow probing Titan’s troposphere, while the surface can be probed only if methane absorption is very small. By ignoring weak methane bands, the RT codes are

quite insensitive to Titan’s troposphere, and may not properly account for Titan’s surface reflectivity.

[17] In order to best characterize the relative contributions from the stratosphere, troposphere and surface we have cleared the haze in the troposphere from the ground up (model 2 above). This effectively removes haze from altitudes not probed in the RT code due to missing methane lines. Any haze present in this region would artificially increase the  $I/F$ , and hence decrease the surface reflectivity obtained by fitting the spectra. By clearing the troposphere we raise, in essence, the surface up in altitude to levels where methane absorption is properly taken into account. The haze is properly distributed throughout the rest of the atmosphere, and the relative contributions from the surface, troposphere/lower stratosphere and stratosphere are as close to reality as any RT code can get. If we use the Huygens haze profile (as 1 above), the tropospheric haze adds significantly to the “observed”  $I/F$ , increasing the relative atmospheric contribution to unrealistically high values (e.g., over 80% in the surface-probing hcont filter).

## 5. Titan’s Atmosphere

### 5.1. Stratosphere: East-West Asymmetry

[18] Titan was near opposition at the time of probe entry, so that the solar phase angle,  $\alpha$ , changed from  $0.05^{\circ}$  up to  $0.4^{\circ}$  during our observations, with the Sun on Titan’s west side (right on figures). Note that the Sun really was about  $180^{\circ}$  away from Titan, though. This timing is ideal to investigate the controversial cause of the observed east-west asymmetries in Titan’s atmosphere: are the asymmetries caused by a solar phase angle effect (i.e., induced by the Sun), or by the presence of an enhancement in the haze density on the morning side? *Roe et al.* [2002a] observed Titan’s stratosphere in October 1999, August 2000, and February 2001, at solar phase angles of  $0.9^{\circ}$  (Sun in the east),  $6.3^{\circ}$  (Sun in the east), and  $6.2^{\circ}$  (Sun in the west), respectively. The sunward limb was always  $\sim 10\%$  brighter than the other side, so the authors concluded that east-west asymmetries are dominated by the solar phase angle effect. However, they could not rule out a possible haze enhancement on the morning side at small phase angles. Such a haze enhancement had been hypothesized by *Coustenis et al.* [2001], who had observed Titan just past opposition, at  $\alpha = 0.5^{\circ}$ , with the Sun in the west; their viewing geometry was thus quite similar to ours. Like *Roe et al.* [2002a] they used filters that probe the lower stratosphere, and noticed (after deconvolution) that the east-limb of Titan was brighter than the west-limb, opposite to that expected from the solar phase angle effect. The authors suggested an enhancement in the haze density in the east, which they attributed to condensation at night. They called this enhancement a “morning fog.” However, fog is a phenomenon that occurs in the troposphere, usually near the ground, while the haze enhancement on Titan is seen in the stratosphere. We therefore refer to it simply as “haze enhancement,” regardless of its origin.

[19] Figure 6 shows images taken through several narrowband filters on 14–17 January, complemented with data on 20 January (Table 2). These filters probe different regions in Titan’s atmosphere, as characterized through the contribution functions in Figure 5. Images in Jcont

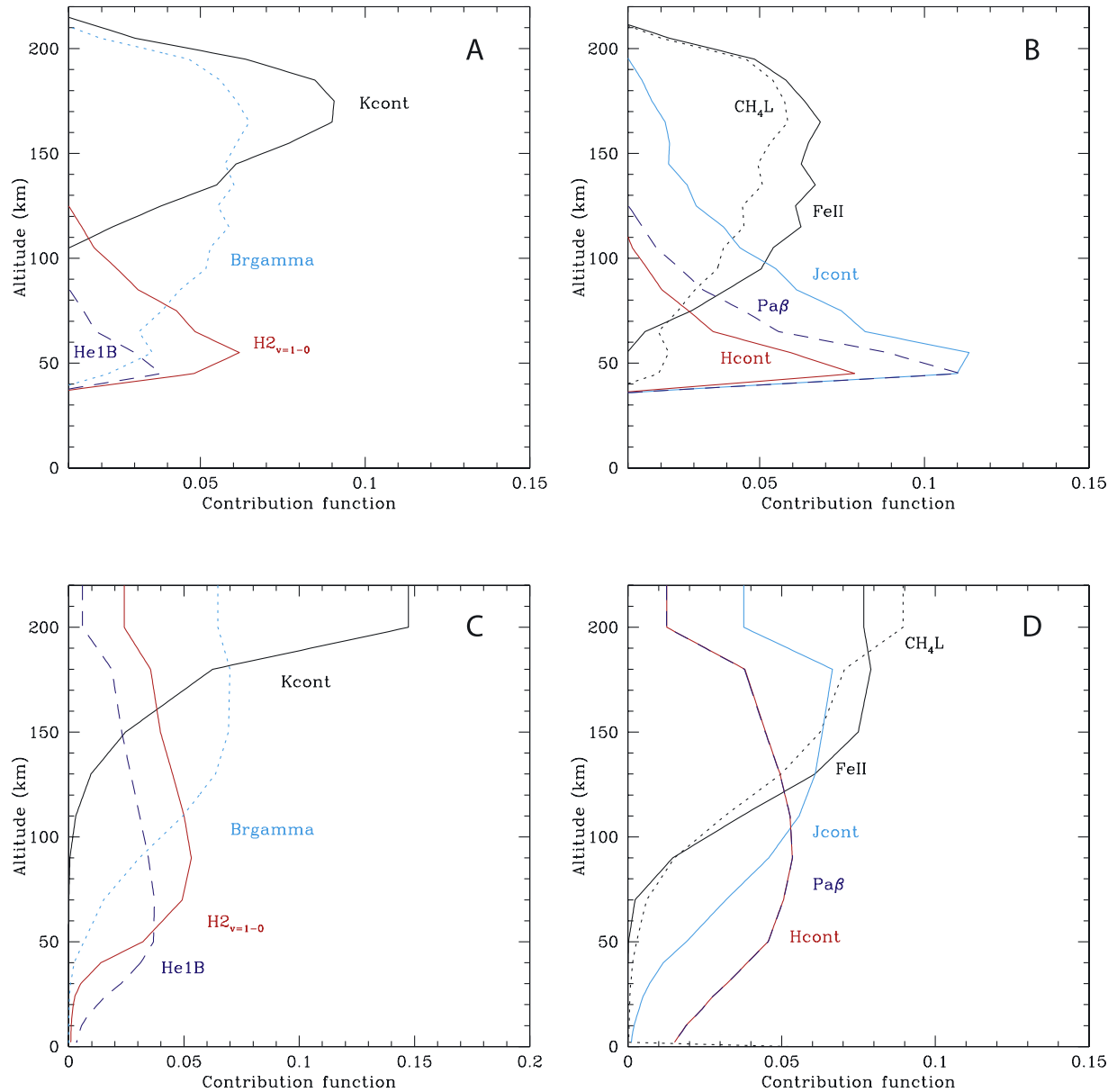


**Figure 5.** Contribution functions for the various narrowband filters used in this paper. We adopted the atmospheric haze profiles that best fit the H band spectral data (Figure 4b). In Figures 5a and 5b we show results for an atmosphere in which the haze has been cleared in the troposphere from the ground up (model 2). In Figures 5c and 5d we used a Huygens-like profile (model 1). The Hcont and Pa $\beta$  profiles in Figure 5d are essentially equal.

and Kcont/CO were only obtained on 15 January. The last column shows 15 January images after deconvolution, which sharpened them significantly. The tropospheric cloud features in the south, as well as the limb brightening in all filters, are clearly visible. Figure 7 shows east-west scans through the original images in Figure 6, sorted by filter, and displaced in  $I/F$  for clarity. These are horizontal (EW) scans at  $15^\circ\text{N}$  latitude. The west (right side = evening) is usually slightly brighter on 15 January, while the east (morning) is brightest on 16–20 January. In  $\text{H}_2 \nu=1-0$  the east side is brightest on 14 January, which switches to the west on 15 January, and then back to the east through 20 January. In the  $\text{CH}_4\text{L}$  filter the west side is brighter than the east side on 14 and 15 January, while the asymmetry is reversed on

16 and 17 January. Similarly, on 15 January the west side is brightest in Bry and FeII, while the east side is brightest on 16–20 January.

[20] In the following we use simple models to calculate the variation in the east/west ratio with solar phase angle, and compare the results with data obtained over the past few years with the 10-m W.M. Keck and 8-m Gemini telescopes. We evaluate the effect on the east/west ratio of (1) Titan’s shadow, (2) extinction of the radiation, (3) scattering by aerosols, and (4) combined extinction and scattering in Titan’s atmosphere.

[21] 1. To investigate the effect of Titan’s shadow on the observations, we built a simple model of a satellite with an atmosphere extending up to 500 km above its surface. We

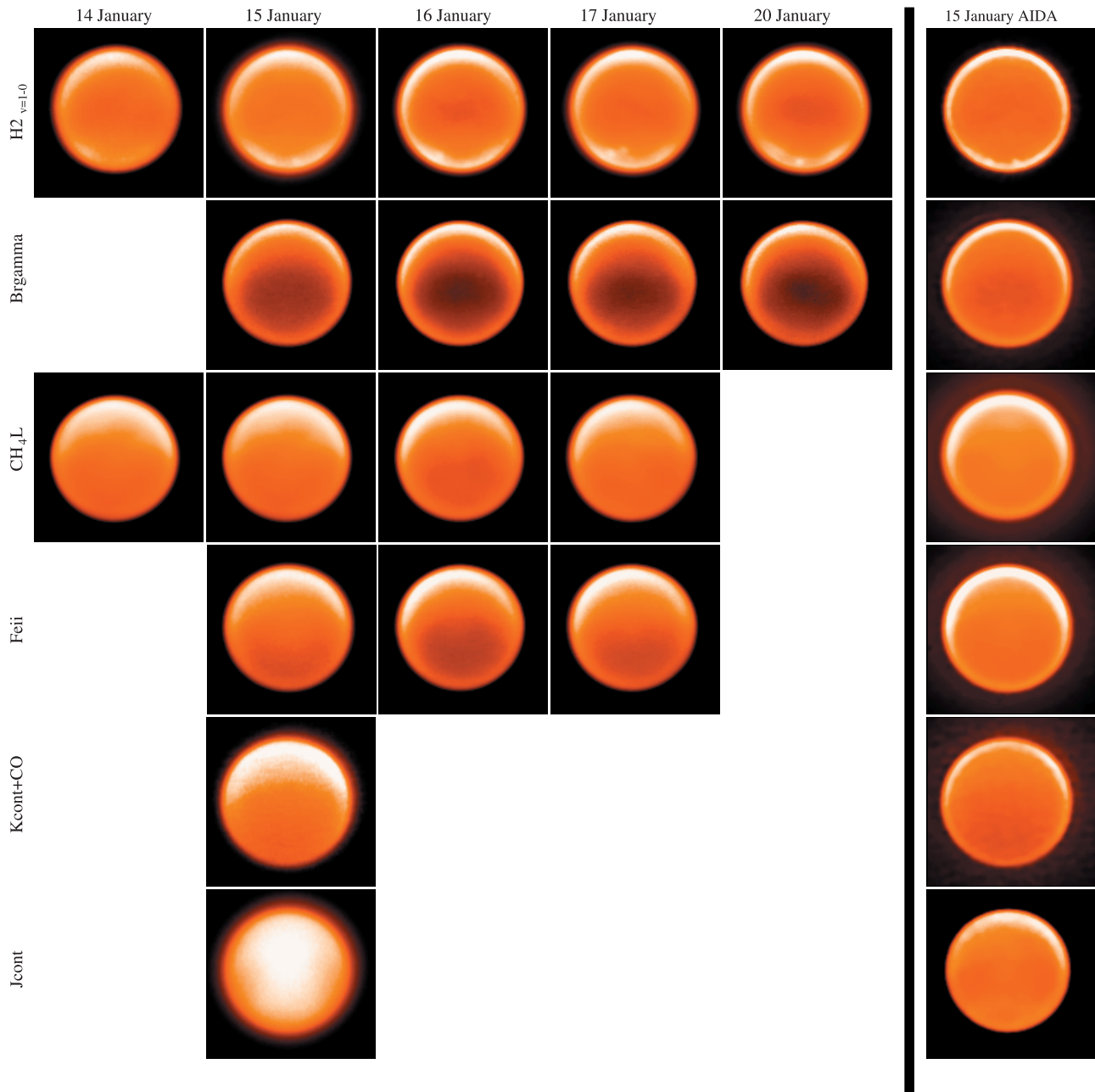


**Figure 6.** Times series of images through different narrowband filters that probe Titan’s atmosphere. The UT date and filter is indicated for each image. The last column shows images from 15 January after deconvolution with AIDA.

assumed that each volume element along the line-of-sight contributes equally to the observed brightness, unless it is in Titan’s shadow, when we assign the volume element a zero brightness (see Figure 8a for a sketch of the geometry). We note that this model includes Titan’s full spherical geometry, and does not depend on the assumption of a plane parallel atmosphere. These calculations are in essence for an optically thin single scattering atmosphere without extinction. The ratio between the morning and evening (called sunlit and “dark” hereafter) limbs is shown by the dotted curve in Figure 8b, for model images with a resolution of  $0.04''$ . A lower (higher) resolution would decrease (increase) the EW asymmetry. At  $\alpha < 0.5^\circ$  there is no phase angle effect; at  $\alpha =$

$1^\circ$  the effect is only 1%. The asymmetry becomes noticeable only at larger phase angles, when a larger fraction of the atmosphere is shadowed by Titan.

[22] 2. In filters that probe Titan’s atmosphere, solar rays will be attenuated more on the dark side, where the path length through the atmosphere is larger (Figure 8a). As in 1, we model Titan’s atmosphere up to 500 km above its surface, and adopt a characteristic extinction profile as retrieved from spectra (Figure 4). We calculate the effect for 4 different filters: Kcont,  $H_{2(v=1-0)}$ , Bry and FeII. As expected, the east-west asymmetries for the three stratosphere probing filters are very similar (one curve shown), while the deeper probing filter ( $H_{2(v=1-0)}$ ) shows a slightly

**Table 2.** Additional Data Used in Figure 9

UT Date	Filters	CML, deg	Phase Angle <sup>a</sup>	Reference <sup>b</sup>
1999-Oct-30	H1702 <sup>c</sup>	109	0.89 E	<i>Roe et al.</i> [2002a]
2000-Aug-17	H1702	208	6.34 E	<i>Roe et al.</i> [2002a]
2001-Jan-11	H1702	285	5.19 W	this paper
2001-Feb-19	H1702	106	6.20 W	this paper
2001-Feb-20	H1702	108	6.19 W	<i>Roe et al.</i> [2002a]
2001-Dec-18	H <sub>2</sub> ( $\nu = 1 - 0$ ), Bry	47	1.74 W	<i>Roe et al.</i> [2002b]
2001-Dec-20	H <sub>2</sub> ( $\nu = 1 - 0$ ), Bry	93	1.97 W	<i>Roe et al.</i> [2002b]
2003-Jan-26	H <sub>2</sub> ( $\nu = 1 - 0$ )	154	4.28 W	this paper
2003-Mar-09	H <sub>2</sub> ( $\nu = 1 - 0$ )	21	6.29 W	this paper
2003-Oct-11	H <sub>2</sub> ( $\nu = 1 - 0$ )	204	6.33 E	Team Keck
2003-Oct-12	H <sub>2</sub> ( $\nu = 1 - 0$ )	227	6.32 E	Team Keck
2003-Nov-11	Bry	186	5.57 E	<i>Schaller et al.</i> [2006]
2003-Nov-12	Bry	208	5.44 E	<i>Schaller et al.</i> [2006]
2003-Nov-13	Bry	231	5.37 E	<i>Schaller et al.</i> [2006]
2003-Nov-14	Bry	254	5.28 E	<i>Schaller et al.</i> [2006]
2003-Nov-18	H <sub>2</sub> ( $\nu = 1 - 0$ ), Bry	344	4.60 E	Team Keck
2003-Nov-29	Bry	230	3.91 E	<i>Schaller et al.</i> [2006]
2003-Dec-10	H <sub>2</sub> ( $\nu = 1 - 0$ ), Bry	121	2.50 E	Team Keck
2003-Dec-15	H <sub>2</sub> ( $\nu = 1 - 0$ ), Bry	232	1.94 E	Team Keck
2003-Dec-17	H <sub>2</sub> ( $\nu = 1 - 0$ ), Bry	277	1.71 E	Team Keck
2003-Dec-18	H <sub>2</sub> ( $\nu = 1 - 0$ ), Bry	300	1.60 E	Team Keck
2003-Dec-24	Bry	74	0.95 E	<i>Schaller et al.</i> [2006]
2003-Dec-25	Bry	97	0.83 E	<i>Schaller et al.</i> [2006]
2003-Dec-26	Bry	120	0.70 E	<i>Schaller et al.</i> [2006]
2003-Dec-27	Bry	142	0.56 E	<i>Schaller et al.</i> [2006]
2004-Jan-10	H <sub>2</sub> ( $\nu = 1 - 0$ ), Bry	98	1.13 W	<i>Schaller et al.</i> [2006]
2004-Sep-02	H <sub>2</sub> ( $\nu = 1 - 0$ ), Bry	17	4.65 E	Team Keck
2004-Sep-28	H <sub>2</sub> ( $\nu = 1 - 0$ ), Bry	240	5.97 E	Team Keck
2004-Oct-02	H <sub>2</sub> ( $\nu = 1 - 0$ ), Bry	331	6.08 E	Team Keck
2004-Oct-03	H <sub>2</sub> ( $\nu = 1 - 0$ )	354	6.11 E	Team Keck
2004-Oct-07	Bry	84	6.45 E	<i>Schaller et al.</i> [2006]
2004-Oct-23	H <sub>2</sub> ( $\nu = 1 - 0$ ), Bry	84	6.30 E	Team Keck
2004-Nov-02	H <sub>2</sub> ( $\nu = 1 - 0$ ), Bry	310	6.10 E	Team Keck
2004-Nov-03	H <sub>2</sub> ( $\nu = 1 - 0$ ), Bry	332	6.13 E	Team Keck
2004-Nov-27	H <sub>2</sub> ( $\nu = 1 - 0$ ), Bry	155	4.90 E	Team Keck
2005-Jan-20	H <sub>2</sub> ( $\nu = 1 - 0$ ), Bry	294	0.772 W	Team Keck
2005-Feb-14	H <sub>2</sub> ( $\nu = 1 - 0$ ), Bry	136	3.51 W	this paper
2005-Feb-15	H <sub>2</sub> ( $\nu = 1 - 0$ ), Bry	159	3.61 W	this paper
2005-Feb-25	H <sub>2</sub> ( $\nu = 1 - 0$ ), Bry	25	4.49 W	Team Keck

<sup>a</sup>Phase angle, and direction of the Sun on the sky (west, east), relative to Titan.

<sup>b</sup>Team Keck data are available at <http://www2.keck.hawaii.edu/science/titan/>.

<sup>c</sup>Wavelength range: 1.67–1.73  $\mu\text{m}$ .

lower sunlit/dark ratio (note that at the limb this filter probes the lower stratosphere rather than troposphere).

[23] 3. We see Titan's atmosphere since aerosols scatter incoming sunlight. To evaluate the effect a change in illumination angle would have on a scattering atmosphere, we made use of *van de Hulst's* [1980] Table 12. This table is constructed for a finite plane-parallel atmosphere, viewed and illuminated under different directions. To estimate the sunlit/dark ratio near the limb of Titan, we choose  $\theta = 60^\circ$ . As shown in Figure 8a,  $\theta_0 > \theta$  on the dark, and  $\theta_0 < \theta$  on the sunlit side. We find that the sunlit/dark ratio for an isotropically scattering atmosphere with total optical depth  $\tau = 2$ , and single scattering albedo,  $\varpi = 0.20$  is essentially equal to the extinction-only curve for the stratosphere. The top dashed line in Figure 8b is for a plane-parallel atmosphere with  $\tau = 2$  and  $\varpi = 0.60$ . The sunlit/dark ratios increase if the aerosols become more reflective (increase in  $\varpi$ ) and/or the haze density increases (increase in  $\tau$ ). If the scattering phase function is changed to a Henyey-Greenstein phase function with asymmetry factor  $g > 0$ , the ratios are smaller [*van de Hulst*, 1980, Table 27]. Although these calculations were performed for a plane parallel atmosphere, we find the results enlightening for our discussion of EW asymmetries.

[24] 4. *Gibbard et al.* [2004] modified *Toon et al.'s* [1989] plane parallel RT code to simulate the absorption, reflection and multiple scattering of photons from Titan's atmosphere and surface (constant albedo), assuming longitudinal symmetry, and a smooth variation in haze density with latitude. This code includes the correction factor of *Tran and Rannou* [2004] to properly model Titan's limb. We used this RT code with the haze parameters as determined by *Gibbard et al.* [1999] to evaluate the variation with solar phase angle. We obtained results very similar to the stratospheric extinction-only model in Figure 8b.

[25] Our calculations in 1–4 show that the east-west asymmetry should increase approximately linearly with  $\alpha$ , up to  $\sim 20\%$  at  $\alpha \approx 6^\circ$  for spatial resolutions of  $\sim 0.04''$ .

[26] Observations are shown in Figure 9. We supplemented our data with Keck AO images at larger phase angles, as tabulated in Table 2. We determined the east/west ratio on each image simply by dividing the peak intensities on the east and west limbs, along a horizontal scan through the center of the image. The 3 central rows were averaged to improve the signal to noise. For the 2001 data we averaged the central 5 rows. The uncertainty was derived from the standard deviation near the center of the disk. The east/west ratio is

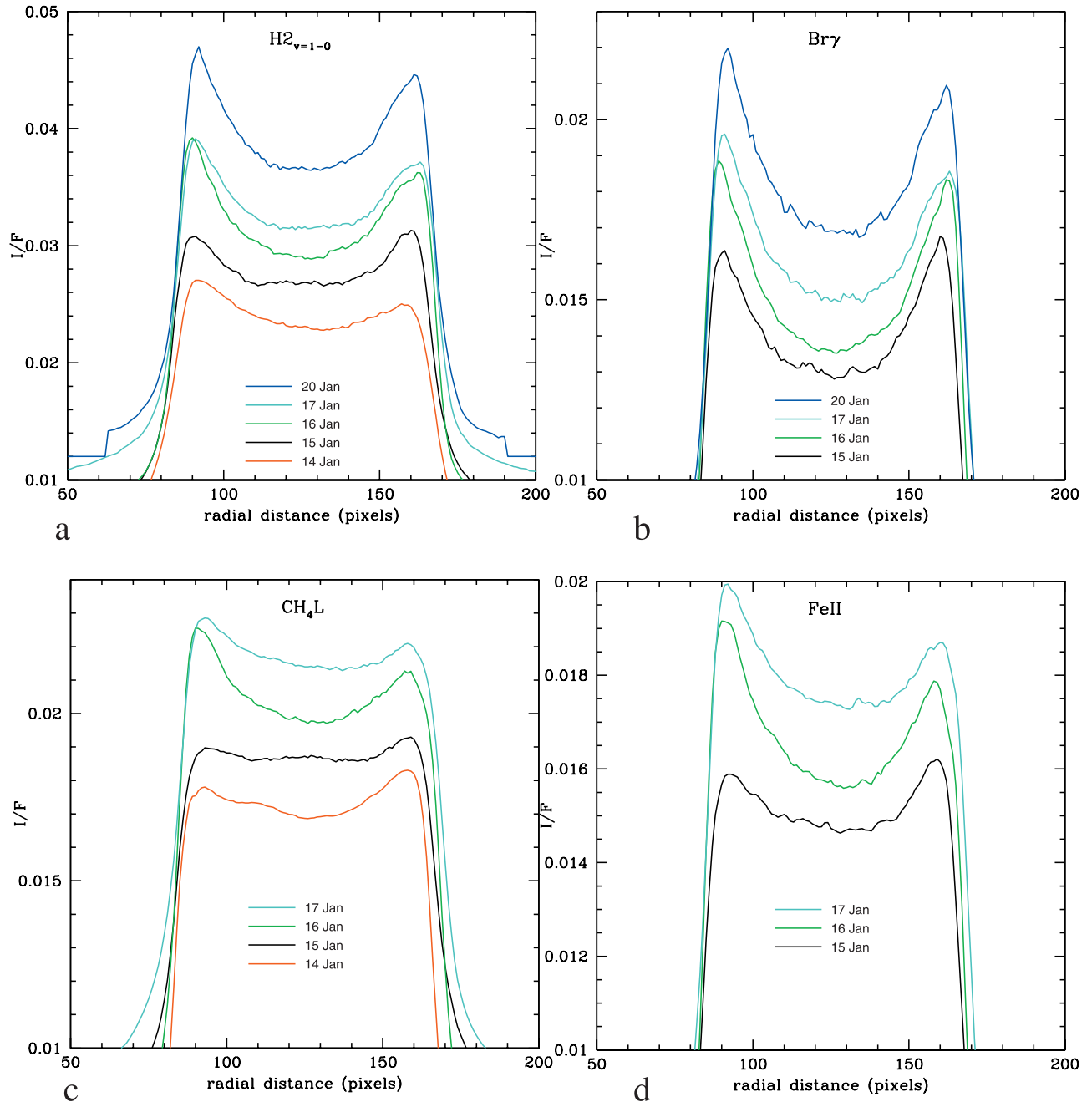


**Figure 7.** East-west (horizontal) scans through all original images from Figure 6. The scans were taken at a latitude of  $\sim 15^\circ$  N (on the central meridian). The lowest profile in each panel corresponds to the profile of the first day, as indicated by the lowermost legend. Profiles on subsequent days are shifted up in  $I/F$ .

plotted as a function of solar phase angle, where we define  $\alpha > 0^\circ$  when the Sun is in the east, and  $\alpha < 0^\circ$  when the Sun is in the west. The solid line shows the Gibbard model, discussed in 4 above. Clearly, most data points lie above the line, indicative of an overall enhancement in haze density on the east or morning side. The dashed line is for a model where the haze density on the east side was arbitrarily increased by 10%.

[27] *Roe et al.* [2005] initiated an intensive observing program at the 8-m Gemini telescope in November 2003, a program that is still ongoing. The observations have been obtained with the NIRI camera coupled to the adaptive optics system [*Hodapp et al.*, 2003], which has a pixel size

of  $0.022''/\text{pixel}$ . These observations span the full range of solar phase angles. Since the spatial resolution is lower than at Keck, we show the Gemini data by themselves in Figure 9b, with overplotted the same Gibbard models at a resolution of  $0.10''$ . These data show the same phenomenon as those in Figure 9a: Most data lie above the solid line, and clearly suggest a several percent enhancement in the haze density on the morning limb.

[28] For both telescopes we showed E/W ratios for different parts in the stratosphere (primarily  $\text{H}_{2(v=1-0)}$  and  $\text{Br}\gamma$  filters). Although on individual days the ratios measured in the two filters are sometimes noticeably different,

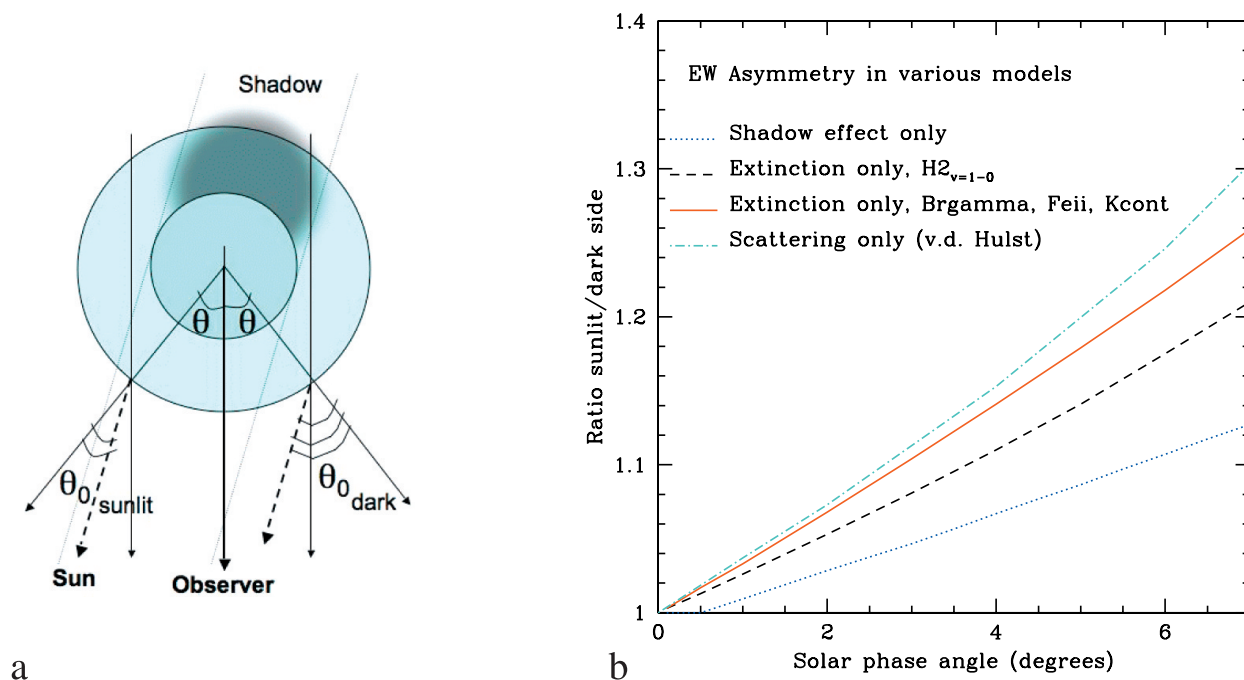


**Figure 8.** (a) Sketch of the geometry for the various calculations. We look down on Titan's orbital plane. The direction to the Sun and the observer, and the angles  $\theta$  (to the observer) and  $\theta_0$  (to the Sun) on both the sunlit and dark side are indicated. (b) Various model results to assess the east-west asymmetry (sunlit/dark side) on Titan as induced by a solar phase angle effect. Full details are given in the text. The dotted blue line (lowest curve) is for a model where only shadowing was considered (atmospheric opacity ignored). The black dashed and red solid lines are models where only extinction in the atmosphere was taken into account. The black dashed line is for a filter probing the troposphere/lower stratosphere, while the red solid line is for the stratosphere. The extinction profile as a function of altitude was taken from the best fit parameters of the Titan H band image data cube (Figure 4). The top (dot-dash cyan curve) line is for a plane parallel atmosphere with isotropic scattering, and a single scattering coefficient  $\varpi = 0.60$ .

we do not see a specific trend between ratios measured in the lower versus upper stratosphere. As mentioned above (Figure 6), there may be asymmetry reversals between images taken through different filters on the same day (e.g., at  $\alpha = 0.05^\circ$  and  $1.13^\circ$ ), and sometimes larger than average day-to-day variations. From the entire collection of data we conclude the following: (1) The E/W ratio is strongly influenced by the solar phase angle effect. (2) The haze tends to be enhanced on the morning side, by up to  $\geq 10\%$ . (3) No clear correlation in E/W asymmetry with altitude has been detected. (4) There may be additional azimuthal inhomogeneities in the haze density. We add a cautionary note here, though. The E/W ratio is strongly affected by the Strehl ratio of the observations. A low ratio tends to equalize the intensities at the limb of the satellite. The overall scatter in the E/W ratios, as well as ratios that are closer to unity than expected at the particular solar phase angle, are likely caused by variations in Strehl ratio. E/W ratios that are exceptionally large (in absolute sense) are harder to attribute to observational problems, although an apparent motion of the object on the sky (due, e.g., to high winds, or starting the integration before the system was completely ready) could influence the observed value. Usually such effects are obvious in the data, and such points were removed prior to plotting.

[29] At this time we cannot give a full explanation for the haze enhancement effect. When *Coustenis et al.* [2001] first

suggested this effect on Titan's morning side, they suggested possible enhanced condensation at night. Indeed, a parcel of air will spend at least a terrestrial day on the night side of Titan, considering that zonal winds usually do not exceed velocities of  $\sim 100\text{--}150$  m/s [e.g., *Moreno et al.*, 2005; *Bird et al.*, 2005]. If the stratosphere is colder then during the day, species may condense out. Whether there is a temperature drop at night, however, remains ambiguous [*Lindal et al.*, 1983; *Coustenis et al.*, 2001]. Regarding possible changes in the EW asymmetry over time, and/or anticorrelations between altitudes, we note that the Cassini spacecraft observed variations in Titan's haze layers over time scales of hours [*Porco et al.*, 2005]. Since the windshear in Titan's stratosphere is strong [*Bird et al.*, 2005], vertical mixing between layers may be small. In addition, cryovolcanism or geysers may supply the atmosphere episodically [*Roe et al.*, 2005], although in our data we do not see any correlation in the EW asymmetry with Titan longitude. This may not be surprising, since we probe well above the tropopause, and vertical mixing between the troposphere and upper stratosphere is not expected.

## 5.2. Troposphere: Clouds and Hazes

[30] As shown in Figure 6, weather on Titan during probe entry and on subsequent days was very quiet. Clouds are most easily spotted in the  $\text{H}_2(\nu=1-0)$  filter (Figure 5) [*Roe et al.*, 2002b]. A small brightening is visible on 14 January in

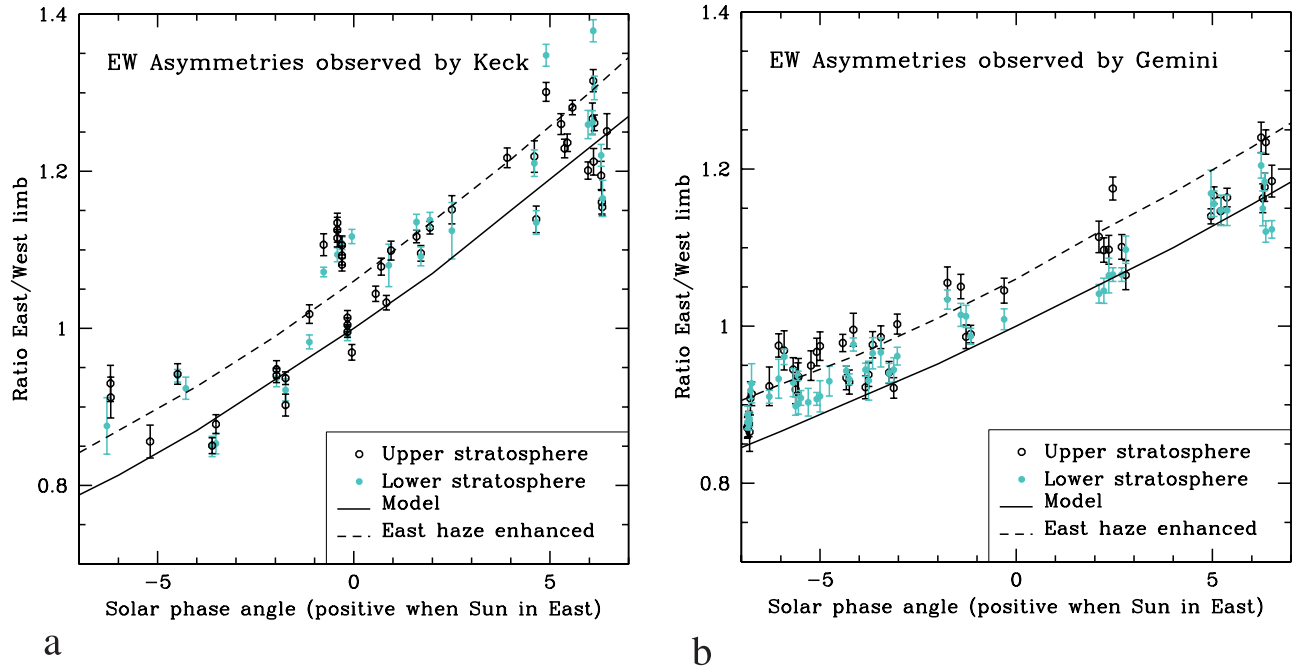


**Figure 9.** Observations of the east-west asymmetry on Titan as a function of solar phase angle. In Figure 9a we show results based on Keck images (see Tables 1 and 2), and in Figure 9b we show results from Gemini data [from *Roe et al.*, 2005]. The solar phase angle was defined positive for the Sun in the east and negative for the Sun in the west. Superposed is the *Gibbard et al.* [1999, 2004] model as discussed in the text. The solid line is for a haze distribution that is homogeneous in longitude, and the dashed line is for hazes enhanced by 10% on the east side.

the south, on the morning hemisphere, which was probably caused by a slight enhancement in the local haze concentration. The next day two small features appeared near the south pole, which became more noticeable on subsequent nights. The quiescent weather may either be fortuitous, or mark a change in weather conditions after the extreme storms in October 2004, as discussed by *Schaller et al.* [2006]. In Figure 10 we show a set of K' band spectra that were taken on and off a small cloud in the south, on 17 January, as indicated by the arrows on the inset, an AIDA deconvolved image in the narrowband  $H_{2(\nu=1-0)}$  filter. The two spectra were taken through the same air mass on Titan. We could best fit the spectra with a cloud at an approximate altitude of 30–40 km, which is similar to the mid-latitude clouds observed by Cassini [*Griffith et al.*, 2005].

[31] The tropospheric haze in the south is clearly visible in both the  $H_{2(\nu=1-0)}$  and Jcont filters, while in both filters the northern hemisphere is dominated by stratospheric haze. In the Jcont filter <20% of the reflected light can be attributed to surface reflectivity near the center of the planet, where the optical depth through the atmosphere is smallest. The tropospheric haze in the south as seen in the  $H_{2(\nu=1-0)}$  filter covers the south polar region up to a latitude of  $\sim 45^\circ\text{S}$ , consistent with the findings by *Roe et al.* [2002b] from images taken in December 2001. At that time, however, there was much more haze near Titan's south pole than at present [*Ádámkóvics et al.*, 2004, 2006]. While the former enhancement may have been caused by sedimentation from higher altitudes, from the time stratospheric haze was still prevalent above the south pole, the more recent measure-

ments may reveal the low latitude return flow in general circulation models [e.g., *Rannou et al.*, 2002] from the north to the south pole.

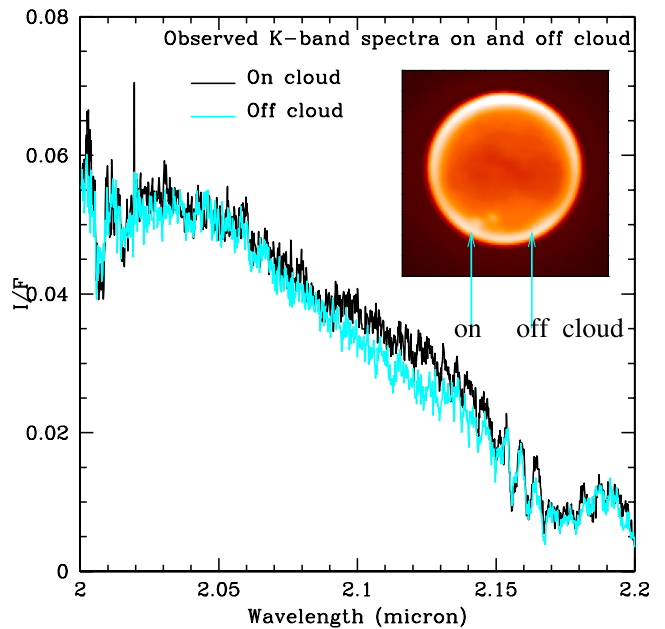


**Figure 10.** K-band spectra from 17 January 2005, taken on and off a cloud feature, at the same Titan air mass. The inset is an AIDA deconvolved image in the narrowband  $H_{2(\nu=1-0)}$  filter. The clouds are clearly visible on this image.

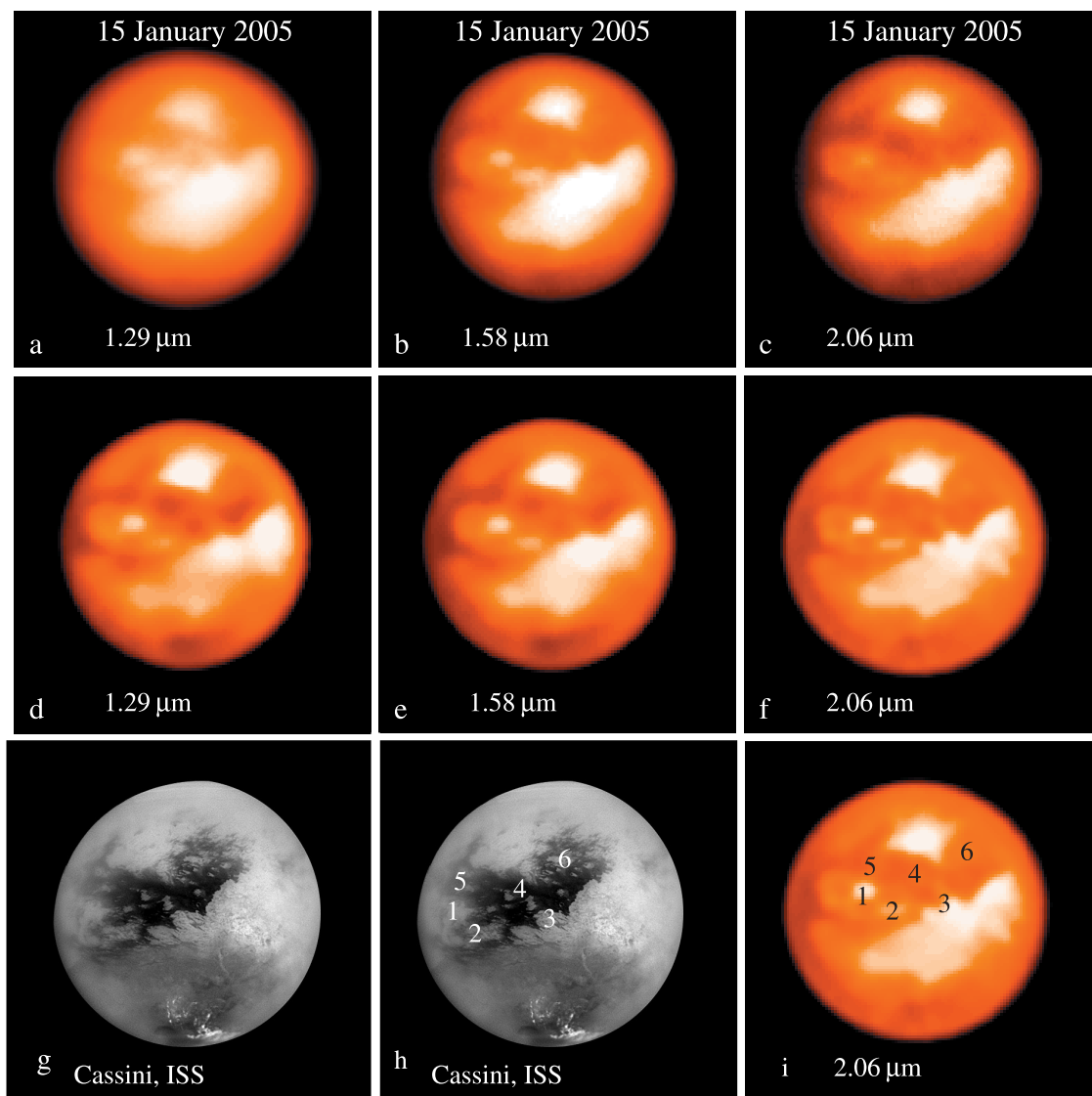


**Figure 11.** Titan's surface viewed through several narrowband filters on 15 January (Pa $\beta$ , Hcont and HeI $\beta$ ) at a central meridian longitude CML = 177°. The top row shows the basic processed images from 15 January; the middle row shows the same data after AIDA deconvolution. In Figure 11g we show a Cassini image taken with the Narrow Angle Camera of the Imaging Science Subsystem at 0.9  $\mu\text{m}$ , taken during Cassini's close approach on 26 October 2004 at a CML = 156°. This mosaic of Titan's surface was made from 16 images (NASA/JPL/Space Science Institute). Figures 11h and 11i highlight similarities between the Cassini and Keck images.

[32] In the Jcont filter the tropospheric structure is markedly different from that in the H<sub>2</sub>( $\nu=1-0$ ) filter (Figure 6, deconvolved), being more like a polar collar than polar cap, centered at a latitude of 60°S. This is quite intriguing and begs for a more in-depth multi-wavelength study in the future. The difference in structure between wavelengths may be caused by a wavelength dependence in aerosol scattering.

## 6. Titan's Surface 1 Day After Probe Entry

[33] Titan's surface is seen in all three broad band filters J, H, and K', but in all three filters there is a significant atmospheric contribution as well. Several of our narrowband filters probe Titan's surface without much contamina-

tion by the atmosphere (section 4 and Figure 5). We show the narrowband surface images from 15 January UT in Figures 11a–11c, with deconvolved images in Figures 11d–11f. As shown, the deconvolution sharpened the images considerably, although all details are also visible on the original images. We note in particular the improvement in the J band image. The original image is rather blurry because of the low Strehl ratio, and hence large PSF halo. AIDA, which solves simultaneously for the best characterization of the object and its PSF, uncovered Titan's fine structure extremely well, as shown. There is excellent agreement in surface structure between the 3 wavelengths, as well as with the Cassini Imaging Science Subsystem (ISS) composite image from the close flyby on 26 October 2004 (Figure 11g), under almost the same viewing angle. In

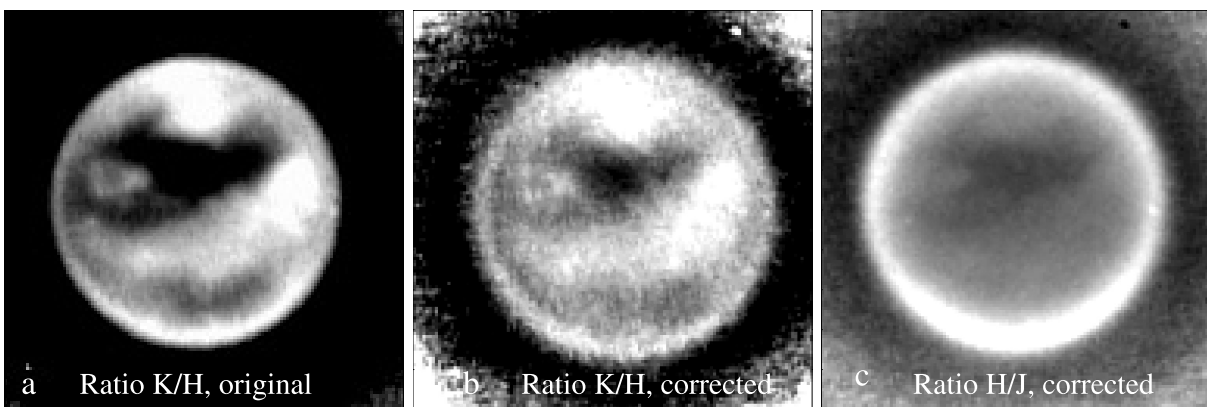


**Figure 12.** Ratioed images: (a) HeI $\beta$ /Hcont from Figures 11a and 11b (see text for discussion). (b) HeI $\beta$ /Hcont after removal of the atmosphere, as discussed in the text. (c) Hcont/Pa $\beta$  after removal of the atmosphere.

Figures 11h and 11i we highlight some of the similarities. Note that in October a bright cloud complex was seen near Titan's south pole, which was absent in January.

[34] Although the images at the three wavelengths look very much alike, interpretation of surface properties, as composition and structure, make it necessary to quantitatively determine the surface albedo and relative contrast between the bright and dark regions at the three wavelengths. If the atmospheric contribution would be zero, one would simply measure the surface albedo directly, and by dividing images one would see how the relative contrast between bright and dark regions would vary between the 3 wavelengths. However, the atmospheric contribution is not zero, and moreover increases with decreasing wavelength. A simple ratio of maps therefore reveals the same dark/bright pattern (Figure 12a) as in the original images, as if the contrast between dark and bright areas is largest at 2.06  $\mu\text{m}$ , and smallest at 1.29  $\mu\text{m}$ .

[35] Ideally, the surface reflectivity and relative contrast between dark and bright areas should be extracted by fitting a full atmosphere–surface coupled model to 3-D image data cubes. *Ádámkóvics et al.* [2006] did this experiment using integral-field spectrometer data from the VLT (SINFONI), obtained simultaneously at H and K bands. Their Figure 7 shows retrieved surface albedos at 5 different locations on Titan's disk, and their Figure 12 shows images of the derived surface reflectivities. As discussed in section 4, the omission of weak methane absorption bands in the models lead to inaccuracies in the derived surface reflectivities. We therefore use the “conventional” method of subtracting an image of Titan's atmosphere from our data to evaluate the relative brightness contrast of the surface between the 3 wavelengths.

[36] Using Hubble Space telescope (HST) data, *Smith et al.* [1996] subtracted images of Titan's atmosphere from broadband data to investigate relative albedo variations across the satellite's surface. By analogy, we subtracted the Jcont image from all three narrowband images, weighted by the relative atmospheric contribution in each filter (section 4 and Figures 5a and 5b; 14% at 2.06  $\mu\text{m}$ , 28% at 1.58  $\mu\text{m}$ , and 43% at 1.29  $\mu\text{m}$ ). This process will not reveal the absolute surface reflectivities, but may retain the proper contrast. After normalizing the resulting images (so each

image  $I/F$  equals unity on average), we ratioed them to one another; results are shown in Figures 12b and 12c. Interestingly enough, the dark/bright contrast as seen in Figure 12a is still clearly visible, although, as expected, at a reduced level. Hence the contrast between dark and bright areas may indeed be larger at 2.06  $\mu\text{m}$  than at H or J band (by up to 10–15%). Similar results were obtained after subtracting Minnaert limb-darkened and limb-brightened disks (using  $\cos^{\pm 1/4}$  dependence).

[37] Since our narrowband JHK images probe Titan's surface in H<sub>2</sub>O-ice absorption bands, our finding of a possibly enhanced dark/bright contrast at 2.06  $\mu\text{m}$  suggests a difference in the absorption characteristics of the surface ice component between the dark and bright areas. Such differences can be caused by the sheer amount of ice, the temperature of the ice, the grain size of frost and whether or not the frost is coating a layer of solid ice. Since low albedo features absorb more sunlight, they will be warmer than their bright counterparts. A difference in bond albedo of 10–20% will only induce a temperature difference of 3–6 K. This leads to changes in absorptivity over our bandwidths of no more than 1–2% [*Grundy and Schmitt*, 1998]. Hence the difference in surface contrast between the various wavelengths cannot be explained by a difference in surface temperature between the dark and bright areas.

[38] Absorption spectra of surface ice change dramatically with grain size and whether or not one probes down to a layer of solid ice. We probably can discard the latter scenario, on the basis of measurements of the dielectric constant by *Elachi et al.* [2005]. They determined a bulk dielectric constant of 2, which is inconsistent with that of solid water ice (3.1), or ammonia ice (4.5), but would be consistent with porous ice and/or an organic sludge. If the frost is fine-grained, scattering predominates and will subdue weak absorption features, in contrast to coarse-grained frost, where absorption dominates [e.g., *Fink and Sill*, 1982]. Perhaps surface frost on the bright terrain consists of finer grains than the frost on Titan's dark terrain, which would lead to a relative decrease in the 1.6  $\mu\text{m}$  absorption feature compared to that at 2.0  $\mu\text{m}$  [*Clark*, 1980]. Such a difference in grain size could be caused by a dark terrain that is, or has been, “wetter” (hydrocarbon slush) in the past. Alternatively, or in addition, it is also feasible that there are

additional absorbers in the dark terrain, such as  $\text{NH}_3$  and/or  $\text{NH}_4\text{SH}$  frost, which absorb more at 2 than at 1.6  $\mu\text{m}$  [Fink and Sill, 1982]. Ammonia was probably present in the form of ammonia hydrates when the satellite formed [Lewis, 1971; Waite *et al.*, 2005], and because ammonia lowers the freezing temperature of water considerably, its presence would readily explain cryovolcanism on Titan. Ironically, no clear evidence for either water or ammonia ice has been found so far.

## 7. Conclusions and Future Prospects

[39] We presented Keck AO data in the form of spectra and narrowband images that were taken during the time the Huygens probe descended through Titan's atmosphere, and on the days following touch-down. The spatial resolution of the images was near the diffraction limit of the telescope,  $\sim 0.04''$  ( $\approx 240$  km on Titan). No entry flash was detected in the data. The atmosphere was relatively clear during probe entry time and on the following days, except for a few small clouds near the south pole, at typical altitudes of 30–40 km. Haze was prominent above the northern hemisphere in the stratosphere, while tropospheric haze was present in the south, shown both in the  $\text{H}_{2(\nu=1-0)}$  and Jcont filters. In the latter filter the haze was distributed in the form of a collar at 60°S. Although the haze is clearly visible in the images, it is much less intense than in 2001. Perhaps we now see the haze resulting from the low altitude return flow in general circulation models [e.g., Rannou *et al.*, 2002], whereas in 2001 most of the haze in this region might have resulted from a slow settling of aerosols from above, from the time the stratospheric haze was still present over the south pole.

[40] Our images of Titan's atmosphere clearly revealed an east-west asymmetry that is not a simple function of solar phase angle. To examine this in detail, we extended our database with images at other phase angles, obtained both with Keck and the Gemini telescopes over the past years. We found a clear dependence in the east-west asymmetry with solar phase angle, but noticed that the haze is usually enhanced on the east side, by up to  $\approx 10\%$ . There may also be azimuthal inhomogeneities in the haze distribution, which sometimes favor the west, other times the east side.

[41] Narrowband images of Titan's surface revealed most of the fine structure seen on Cassini ISS images, in particular after deconvolution with AIDA. After correcting the images to first order for Titan's atmosphere, the dark/bright surface contrast at 2  $\mu\text{m}$  may be larger than that at 1.6 and 1.3  $\mu\text{m}$ , indicative perhaps of coarser-grained frost in the dark areas compared to the bright regions, and/or the presence of additional absorbers in these dark areas.

[42] *Future:* Continued ground-based observations play a crucial role in the ultimate understanding of Titan's meteorology. We still do not have a good understanding of the mechanisms for formation, evolution and loss of haze particles, nor the significance of how aerosols contribute to the global atmospheric circulation. To improve existing theories, we need to observe the time-dependent spatial and vertical distribution of Titan's haze over a full Titan year (30 Earth years). Such long programs can only be carried out with ground-based telescopes, since space missions are typically too limited in extent (and funding). At present the Cassini mission will be in orbit for only  $\sim 1.5$  Titan months,

and the Huygens probe sampled just one moment in Titan's history, at one location. Hence, to complement and extend the Cassini/Huygens mission we encourage ground-based observers to continue to observe. Moreover, with recent advances in detector technology, such as the field-integral spectrometers SINFONI on the VLT and OSIRIS on Keck, we can now obtain image data cubes of the satellite within 1/2 hour, and convert these into 3-D haze profiles.

[43] Neither ground-based data nor the Cassini/Huygens mission have identified liquid hydrocarbons on Titan's surface, although the surface topology clearly hints at the presence of liquids in the past. Methane gas in Titan's atmosphere requires an efficient recycling mechanism, akin either to the hydrological cycle on Earth or perhaps via active cryovolcanism or geysers. Lorenz *et al.* [2005] remarked that rainstorms on Titan are rare, but perhaps extremely violent. Will we ever witness such storms? Only time and continued observations can tell.

[44] **Acknowledgments.** This work was funded by the National Science Foundation and Technology Center for Adaptive Optics, managed by the University of California at Santa Cruz under cooperative agreement AST-9876783, and by the Center for Integrative Planetary Science at the University of California in Berkeley. The research was further funded through UCB grants AST-0205893 from the National Science Foundation and NNG05GH63G from NASA. S.G.'s work was performed under the auspices of the U.S. Department of Energy, National Nuclear Security Administration by the University of California, Lawrence Livermore National Laboratory under contract W-7405-Eng-48. The data presented in this paper were obtained at the W. M. Keck Observatory, which is operated as a scientific partnership among the California Institute of Technology, the University of California, and the National Aeronautics and Space Administration. The Observatory was made possible by the generous financial support of the W. M. Keck Foundation. The authors wish to recognize and acknowledge the very significant cultural role and reverence that the summit of Mauna Kea has always had within the indigenous Hawaiian community. We are most fortunate to have the opportunity to conduct observations of Titan from this Hawaiian volcano.

## References

- Ádámkóvics, M., I. de Pater, H. G. Roe, S. G. Gibbard, and C. A. Griffith (2004), Spatially-resolved spectroscopy at 1.6  $\mu\text{m}$  of Titan's atmosphere and surface, *Geophys. Res. Lett.*, *31*, L17S05, doi:10.1029/2004GL019929.
- Ádámkóvics, M., I. de Pater, F. Eisenhauer, M. Hartung, R. Genzel, and C. Griffith (2006), Titan's bright spots: Multiband spectroscopic measurement of surface diversity and hazes, *J. Geophys. Res.*, doi:10.1029/2005JE002610, in press.
- Bird, M. K., et al. (2005), The vertical profile of winds on Titan, *Nature*, *438*, 800–802.
- Clark, R. N. (1980), Ganymede, Europa, Callisto, and Saturn's rings—Compositional analysis from reflectance spectroscopy, *Icarus*, *44*, 388–409.
- Colina, L., R. C. Bohlin, and F. Castelli (1996a), The 0.12–2.5 micron absolute flux distribution of the sun for comparison with solar analog star, *Astron. J.*, *112*, 307–315.
- Colina, L., R. C. Bohlin, and F. Castelli (1996b), Absolute flux calibration spectrum of Vega, *Instrum. Sci. Rep. OSG-CAL-96-01*, Space Telescope Sci. Inst., Baltimore, Md.
- Coustonis, A., E. Gendron, O. Lai, J.-P. Véran, J. Woillez, M. Combes, L. Vapillon, T. Fusco, L. Mugnier, and P. Rannou (2001), Images of Titan at 1.3 and 1.6  $\mu\text{m}$  with adaptive optics at the CFHT, *Icarus*, *154*, 501–515.
- de Pater, I., S. G. Gibbard, and H. B. Hammel (2006), Evolution of the dusty rings of Uranus, *Icarus*, *180*, 186–200.
- Elachi, C., et al. (2005), Cassini radar views the surface of Titan, *Science*, *308*, 970–974.
- Elias, J. H., J. A. Frogel, K. Matthews, and G. Neugebauer (1982), Infrared standard stars, *Astron. J.*, *87*, 1029–1034.
- Fink, U., and G. T. Sill (1982), The infrared and spectral properties of frozen volatiles, in *Comets*, edited by L. L. Wilkening, pp. 164–202, Univ. of Ariz. Press, Tucson.
- Fulchignoni, M., et al. (2005), In situ measurements of the physical characteristics of Titan's environment, *Nature*, *438*, 785–791, doi:10.1038/nature04314.

- Gibbard, S. G., B. Macintosh, D. Gavel, C. E. Max, I. de Pater, A. M. Ghez, E. F. Young, and C. P. McKay (1999), Titan: High resolution speckle images from the Keck telescope, *Icarus*, *139*, 189–201.
- Gibbard, S. G., I. de Pater, B. A. Macintosh, H. G. Roe, C. E. Max, E. F. Young, and C. P. McKay (2004), Titan's 2  $\mu\text{m}$  surface albedo and haze optical depth in 1996–2004, *Geophys. Res. Lett.*, *31*, L17S02, doi:10.1029/2004GL019803.
- Griffith, C. A., et al. (2005), The evolution of Titan's mid-latitude clouds, *Science*, *310*, 474–477.
- Grundy, W. M., and B. Schmitt (1998), The temperature-dependent near-infrared absorption spectrum of hexagonal H<sub>2</sub>O ice, *J. Geophys. Res.*, *103*, 25,809–25,822.
- Hodapp, K. W., et al. (2003), The Gemini Near-Infrared Imager (NIRI), *Publ. Astron. Soc. Pac.*, *115*, 1388.
- Irwin, P. G. J., K. Sihra, N. Bowles, F. W. Taylor, and S. B. Calcutt (2005), Methane absorption in the atmosphere of Jupiter from 1800 to 9500  $\text{cm}^{-1}$  and implications for vertical cloud structure, *Icarus*, *176*, 255–271.
- Lellouch, E., A. Coustenis, D. Gautier, F. Raulin, N. Dubouloz, and C. Frere (1989), Titan's atmosphere and hypothesized ocean—A reanalysis of the Voyager 1 radio-occultation and IRIS 7.7-micron data, *Icarus*, *79*, 249–328.
- Lewis, J. S. (1971), Satellites of the outer planets: Their physical and chemical nature, *Icarus*, *15*, 174–185.
- Lindal, G. F., G. E. Wood, H. B. Hotz, D. N. Sweetnam, V. R. Eshleman, and G. L. Tyler (1983), The atmosphere of Titan—An analysis of the Voyager 1 radio occultation measurements, *Icarus*, *53*, 348–363.
- Lorenz, R. D. (2002), Huygens Probe: An artificial meteor on Titan?, *Astron. Geophys.*, *43*, 5.14–5.18.
- Lorenz, R. D., C. A. Griffith, J. I. Lunine, C. P. McKay, and N. O. Rennó (2005), Convective plumes and the scarcity of Titan's clouds, *Geophys. Res. Lett.*, *32*, L01201, doi:10.1029/2004GL021415.
- Lorenz, R. D., et al. (2006), Huygens entry emission: Observations campaign, results, and lessons learned, *J. Geophys. Res.*, doi:10.1029/2005JE002603, in press.
- McKay, C. P., A. Coustenis, R. E. Samuelson, M. T. Lemmon, R. D. Lorenz, M. Cabane, P. Rannou, and P. Drossart (2001), Physical properties of the organic aerosols and clouds on Titan, *Planet. Space Sci.*, *49*, 79–99.
- Moreno, R., A. Marten, and T. Hidayat (2005), Interferometric measurements of zonal winds on Titan, *Astron. Astrophys.*, *437*, 319–328.
- Mugnier, L. M., T. Fusco, and J.-M. Conan (2004), MISTRAL: A myopic edge-preserving image restoration method, with application to astronomical adaptive-optics-corrected long-exposure images, *Opt. Soc. Am. J.*, *21*, 1841–1854.
- Porco, C. C., et al. (2005), Imaging of Titan from the Cassini spacecraft, *Nature*, *434*, 159–168.
- Rannou, P., F. Hourdin, and C. P. McKay (2002), A wind origin for Titan's haze structure, *Nature*, *418*, 853–856.
- Roe, H. G., I. de Pater, B. A. Macintosh, S. G. Gibbard, C. E. Max, and C. P. McKay (2002a), Note: Titan's atmosphere in late southern spring observed with adaptive optics on the W. M. Keck II 10-meter telescope, *Icarus*, *157*, 254–258.
- Roe, H. G., I. de Pater, B. A. Macintosh, and C. P. McKay (2002b), Titan's clouds from Gemini and Keck adaptive optics imaging, *Astrophys. J.*, *581*, 1399–1406.
- Roe, H. G., M. E. Brown, E. L. Schaller, A. H. Bouchez, and C. A. Trujillo (2005), Geographic control of Titan's mid-latitude clouds, *Science*, *310*, 477–479.
- Rousselot, P., C. Lidman, J.-G. Cuby, G. Moreels, and G. Monnet (2000), Night-sky spectral atlas of OH emission lines in the near-infrared, *Astron. Astrophys.*, *354*, 1134–1150.
- Schaller, E. L., M. E. Brown, H. G. Roe, A. H. Bouchez, and C. A. Trujillo (2006), Dissipation of Titan's south polar clouds, *Icarus*, in press.
- Smith, P. H., M. T. Lemmon, R. D. Lorenz, L. A. Sormovsky, J. J. Caldwell, and M. D. Allison (1996), Titan's surface, revealed by HST imaging, *Icarus*, *119*, 336–349.
- Tomasko, M. G., et al. (2005), Rain, winds and haze during the Huygens probe's descent to Titan's surface, *Nature*, *438*, 765–778.
- Toon, O. B., C. P. McKay, T. P. Ackerman, and K. Santhanam (1989), Rapid calculation of radiative heating rates and photodissociation rates in inhomogeneous multiple scattering atmospheres, *J. Geophys. Res.*, *94*, 16,287–16,301.
- Tran, T. T., and P. Rannou (2004), Comparing 3D spherical Monte-Carlo and 2-stream parallel plane simulation of far-field backscattering image of Titan, *Notes Pôle Planétol. Inst. Pierre Simon Laplace*, *2*, pp. 18–38, Gif sur Yvette, France.
- Van de Hulst, H. C. (1980), *Multiple Light Scattering: Tables, Formulas and Applications*, Vol. 1 and 2, Elsevier, New York.
- Waite, J. H., et al. (2005), Ion neutral mass spectrometer results from the first flyby of Titan, *Science*, *308*, 982–986.

---

M. Ádámkóvics, I. de Pater, and F. Marchis, Department of Astronomy, University of California, 601 Campbell Hall, Berkeley, CA 94720, USA. (imke@astro.berkeley.edu)

A. H. Bouchez, Caltech Optical Observatories, California Institute of Technology, Pasadena, CA 91125, USA.

M. E. Brown, H. G. Roe, and E. L. Schaller, Division of Geological and Planetary Sciences, California Institute of Technology, Pasadena, CA 91125, USA.

S. G. Gibbard, Lawrence Livermore National Laboratory, Livermore, CA 94550, USA.

E. Young, Southwest Research Institute, Boulder, CO 80302, USA.